Chapter 11
Phase Field Models for Two-Phase Flow with Surfactants and Biomembranes

Sebastian Aland

Abstract We give an overview on recent developments of phase field models for two-phase flows with surfactants and lipid bilayer membranes. Starting from the two-phase flow model of a clean fluid-fluid interface we discuss the time discretization and boundary conditions for dynamic and static contact angles. Using the adsorption models of Henry and Langmuir, soluble surfactants are included in the diffuse interface formulation. To consider lipid bilayer membranes the model is extended by membrane bending stiffness and membrane inextensibility. We present phase field models to include these elastic effects, with a particular focus on the inextensibility constraint for which we discuss different phase field variants from the literature and present numerical tests.

11.1 Introduction

A large collection of fluid problems involve moving interfaces. The simplest examples include everyday phenomena, such as when pouring water in an empty glass filled with ambient air. While the dynamics at the interface between water and air are mostly governed by surface tension, things become more subtle if molecules of an additional chemical species are present at the interface. Such species can range from single surfactant molecules that locally lower the surface tension, to dense structures of elastic lipid molecules that completely isolate the two fluids from each other.

Many numerical techniques are available to handle such two-phase flow problems with additional interfacial particles [48, 49, 59, 60]. One of the simplest and most flexible among these is the phase field (or diffuse interface) method. The method has a sound physical background and can easily handle topological changes of the fluid phases, as well as contact of the fluids with a solid body (or boundary).

In this chapter, we give an overview on recent developments of phase field models for two-phase flow with interfacial particles, be it surfactants or lipid

S. Aland (✉)

Institute of Scientific Computing, TU Dresden, 01062 Dresden, Germany
e-mail: sebastian.aland@tu-dresden.de

molecules. Both cases can be handled quite similar by additional surface and bulk equations and their coupling to the flow dynamics. We start in Sect. 11.2 with the two phase flow model of a clean fluid-fluid interface and discuss the time discretization and boundary conditions for dynamic and static contact angles. Then, we include soluble surfactants and focus on the adsorption models of Henry and Langmuir. In Sect. 11.3 we switch to fluidic membranes where surfactants are replaced by a dense layer of lipid molecules. These molecules give rise to elastic properties, in particular bending stiffness and membrane inextensibility. We present phase field models to include these elastic effects, with a particular focus on the inextensibility constraint. We present different modeling approaches to include this constraint in phase field models and compare them in numerical tests.

11.2 The Diffuse Interface Model for Two Phase Flow with Surfactants

We consider isothermal, incompressible flow of two immiscible fluids. The interface between both fluids is usually considered as a free boundary that evolves in time. Instead of explicitly tracking the fluid-fluid interface, the phase field method uses an auxiliary function (the phase field) and the interface position is implicitly described by a level-set of this function. As opposed to the level-set method, the phase field ϕ takes distinct values in each of the fluid phases (e.g. $\phi = -1$ and $\phi = 1$) with a smooth transition in between, around the interface. Hence, the interface is diffuse with a finite width and an intermediate level set of the phase field (e.g. $\phi = 0$) may be used to get a discrete interface location. Figure 11.1 illustrates the corresponding sharp and diffuse interface settings.

A fine computational grid is needed to numerically resolve the transition layer of thickness ε, which makes phase field computations often more expensive than other interface capturing methods. On the other hand, phase field methods offer
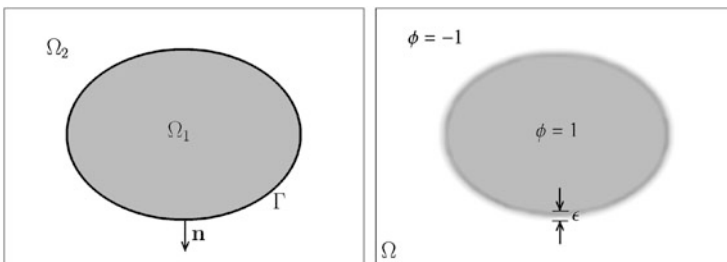
Fig. 11.1 Comparison of a sharp interface model (*left*) with a diffuse interface model (*right*). In the diffuse interface model the domains Ω_1, Ω_2 are implicitly defined by regions where $\phi \approx 1$, $\phi \approx -1$, respectively. The interface Γ is smeared out to an interface region of finite thickness ε, where $-1 < \phi < 1$

many advantages in the mathematical modeling. One distinct advantage is their simplicity. As opposed to Level-Set methods, mass is conserved and reinitialization or convection stabilization are not necessary for the interface advection. Phase field methods naturally admit physical energy laws which makes it possible to develop energy stable discretization schemes. Also topological changes, such as during vesicle fission and fusion, are naturally captured and additional physical processes can be easily included within the phase field formulation.

11.2.1 Phase Field Equations

Given a sharp interface Γ, the surface energy of a fluid-fluid interface can be written as

$$E_s = \int_\Gamma \sigma \, \mathrm{dA}, \tag{11.1}$$

where σ is the surface tension. Van der Waals was the first who realized that real interfaces are not sharp but diffuse with a finite thickness [53]. Based on physical arguments, Cahn and Hilliard [16] formulated the diffuse interface version of a fluid-fluid interface,

$$\tilde{E}_s = \int_\Omega \tilde{\sigma} \left(\frac{\varepsilon}{2} |\nabla \phi|^2 + \frac{1}{\varepsilon} W(\phi) \right) \mathrm{dV}, \tag{11.2}$$

where $\tilde{\sigma} = 3\sigma/2\sqrt{2}$ is a scaled surface tension. The scaling factor depends on the chosen double-well potential W, which is here $W(\phi) = \frac{1}{4}(\phi^2 - 1)^2$.

Hohenberg and Halperin [36] were the first to couple the idea of a diffuse interface to flow dynamics. The simplest form of the resulting Navier-Stokes-Cahn-Hilliard equations is,

$$\rho \partial_t^\bullet \mathbf{v} + \nabla p - \nabla \cdot \left(\eta (\nabla \mathbf{v} + (\nabla \mathbf{v})^T) \right) = -\varepsilon \nabla \cdot (\tilde{\sigma} \nabla \phi \otimes \nabla \phi) + \mathbf{F}, \tag{11.3}$$

$$\nabla \cdot \mathbf{v} = 0, \tag{11.4}$$

$$d_t^\bullet \phi = \nabla \cdot (M(\phi) \nabla \mu), \tag{11.5}$$

$$\mu = \frac{1}{\varepsilon} W'(\phi) - \varepsilon \Delta \phi. \tag{11.6}$$

Here $\mathbf{v}, p, \mu$ and $\mathbf{F}$ are the (volume-averaged) velocity, pressure, chemical potential and body force, respectively. The parameter ε defines the interface thickness, $\partial_t^\bullet = \partial_t + \mathbf{v} \cdot \nabla$ is the material derivative. The term $-\varepsilon \nabla \cdot (\tilde{\sigma} \nabla \phi \otimes \nabla \phi)$ provides the surface tension force, many other forms of this term are possible, see, e.g., [40].

The density $\rho(\phi)$ and viscosity $\eta(\phi)$ are interpolations of the corresponding values in the two fluids, e.g.

$$\rho(\phi) = \rho_1(1 + \phi)/2 + \rho_2(1 - \phi)/2, \qquad \eta(\phi) = \eta_1(1 + \phi)/2 + \eta_2(1 - \phi)/2 \tag{11.7}$$

The Mobility $M(\phi)$ The function $M(\phi)$ is a mobility. In practice, M is often either a constant or a double well potential similar to W. In general for the diffuse interface fluid method, it is desirable to keep M small such that the interface position is primarily advected. At the same time the mobility needs to be big enough to ensure that the interface profile stays accurately modeled and the interface thickness is approximately constant. Asymptotic analysis [1] and numerical benchmarks [6] show that this can be achieved by taking $M = \mathscr{O}(\varepsilon)$.

Non-matched Densities For matched densities, i.e., $\rho_1 = \rho_2$, the above system is thermodynamically consistent, i.e., there exist physical energy estimates. This property is not maintained for non-matched densities ($\rho_1 \neq \rho_2$) which has led to different extensions of the model [1, 15, 45]. The model described in [1] involves an additional term in the momentum equation. The model in [45], defines **v** as the mass-average of the two fluid velocities, which leads to a relaxed incompressibility condition around the interface. However, in many practical applications, the physical interface thickness is very small compared to the domain size. In this case the diffuse interface model aims to approximate the sharp interface solution and the interface thickness ε needs to be chosen very small. For small ε the error introduced by the diffuse interface itself becomes larger than the differences between the various diffuse interface models [6]. In this case, the different diffuse-interface models provide equally good approximations to the sharp-interface solution.

11.2.2 Boundary Conditions

The boundary conditions to the above defined system are particularly interesting when $\partial\Omega$ is a solid boundary. In this case the fluid-fluid interface may touch the solid wall which leads to a moving contact line problem [5]. The Generalized-Navier-Boundary-Condition (GNBC) holds for the fluid velocity [50]

$$\left[l(\phi)(\mathbf{v} - \mathbf{v}_{\text{wall}}) + \eta(\phi)(\nabla\mathbf{v} + \nabla\mathbf{v}^T) \cdot \mathbf{n}_\Omega - L(\phi)\nabla\phi\right] \times \mathbf{n}_\Omega = 0. \tag{11.8}$$

Here $l(\phi)$ is the phase-dependent inverse of the slip length, $\mathbf{v}_{\text{wall}}$ is the wall velocity, $\mathbf{n}_\Omega$ is the outer normal to $\partial \Omega$. The function $L(\phi)$ is defined as

$$L(\phi) = \frac{3\sigma}{2\sqrt{2}} \varepsilon \, \mathbf{n}_\Omega \cdot \nabla \phi - \gamma'(\phi), \tag{11.9}$$

where $\gamma'(\phi)$ is the first derivative of the fluid-wall energy potential

$$\gamma(\phi) = \frac{\sigma}{2} \cos(\theta) \sin(\frac{\pi}{2}\phi), \tag{11.10}$$

with the equilibrium contact angle θ. Note, that γ describes the energy density associated with a fluid touching the wall. In particular, the difference in γ between the two phases is $\gamma(1) - \gamma(-1) = \sigma \cos(\theta)$, which is the difference in the wall energies of fluid 1 and fluid 2, respectively, due to Young's law, $\sigma \cos(\theta) = \sigma_1 - \sigma_2$. The different wall potential $\gamma(\phi) = \sigma \, \cos(\theta) \, (3\phi - \phi^3)/4$ has been used in [7, 56], which leads to equal static contact angles for all level-sets of the phase field [2].

Additionally, the movement of the contact line is determined by the dynamic contact line boundary condition [37, 50]

$$\partial_t \phi + \mathbf{v} \cdot \nabla \phi = -\beta L(\phi) \quad \text{(dynamic angle BC)}, \tag{11.11}$$

for a relaxation parameter β. Hence, the actual contact angle is dynamic and relaxes to the equilibrium angle θ with a speed controlled by β. If this relaxation is very fast, i.e. $\beta \to \infty$, Eq. (11.11) reduces to $L(\phi) = 0$ which implies the following two boundary conditions from Eqs. (11.8), (11.9):

$$\left[l(\phi)(\mathbf{v} - \mathbf{v}_{\text{wall}}) + \eta(\phi)(\nabla \mathbf{v} + \nabla \mathbf{v}^T) \cdot \mathbf{n}_\Omega \right] \times \mathbf{n}_\Omega = 0 \quad \text{(Navier BC)}, \tag{11.12}$$

$$\frac{3\sigma}{2\sqrt{2}} \varepsilon \mathbf{n}_\Omega \cdot \nabla \phi = \gamma'(\phi) \quad \text{(static angle BC)}. \tag{11.13}$$

If additionally the slip length is close to zero, i.e., $l(\phi) \to \infty$, the Navier condition reduces to the common no slip condition

$$\mathbf{v} = \mathbf{v}_{\text{wall}} \quad \text{(no slip BC)}. \tag{11.14}$$

To close the system and to ensure conservation of fluid masses, a no flux condition is specified for the chemical potential,

$$\mathbf{n}_\Omega \cdot \nabla \mu = 0. \tag{11.15}$$

11.2.3   Numerical Discretization

Most numerical methods for the Navier-Stokes-Cahn-Hilliard system (11.3)–(11.6) focus on the no slip boundary condition with no contact lines or a static 90° contact angle, i.e., $\mathbf{n}_\Omega \cdot \nabla \phi = 0$. In this case a lot of different discretization techniques are available for the individual subsystems, see, for example, [38, 51] for Navier-Stokes and [14, 31, 58] for the Cahn-Hilliard system.

Coupling Between Navier-Stokes and Cahn-Hilliard Only in recent years, efficient discretization techniques have been proposed for the coupled Navier-Stokes-Cahn-Hillard system [26, 39]. For small capillary numbers, the surface tension force introduces a strong coupling between the Navier-Stokes equation providing the flow field and the Cahn-Hilliard equation evolving the phase field. In [3] it was shown by numerical tests, that an explicit coupling of these two problems can result in a time step restriction of the form

$$dt_{\max} \lesssim \varepsilon \rho^{2/3} M^{1/3} \sigma^{-1/3}, \tag{11.16}$$

where dt is the time step and M and ρ are assumed to be constant. In contrast to other numerical models for two-phase flow, this time step restriction is independent of the grid size but strongly dependent on ε. It is suspected that this dependence is a consequence of the smallest capillary wavelength that can be resolved in a diffuse interface model. Given the grid resolution is high enough to resolve the diffuse interface properly, this wavelength is proportional to the interface thickness and independent of the grid size. Special techniques have been introduced in [3] to lift the time step constraint, including additional stabilizing terms as well as monolithic coupling of both subproblems. Apart from increasing the computational performance, such improved time integration schemes allow to choose lower mobility, which reduces the non-physical interface movement due to the Cahn-Hilliard dynamics.

Energy-Stable Schemes One advantage of phase field models is that they admit physical energy laws which makes it possible to develop energy stable discretization schemes. Energy stable schemes for the fully discrete Navier-Stokes-Cahn-Hilliard system have been proposed, both in linear form [28] and nonlinear form [29, 30]. Liu et al. [44] also presented an energy stable scheme where the Navier-Stokes and Cahn-Hilliard system are completely decoupled during the solution process. For a modified energy law, even second order convergence in time could be established [32].

Energy stable schemes for the moving contact line problem with the Generalized-Navier-Boundary-Condition have been proposed in [33]. A linear scheme was developed in [5] which enables a very robust unconditionally energy-stable approximation of the Navier-Stokes-Cahn-Hilliard system.

11.2.4 Inclusion of Surfactants

Surfactants are amphiphilic molecules that tend to adsorb at fluid-fluid interfaces. Their presence lowers the surface tension locally and thus has a significant effect on the flow dynamics. A relation between the surfactant concentrations and the local surface tension is given by Gibbs adsorption equation. Let c_1, c_2, c_Γ the surfactant concentrations in phase 1, phase 2 and on the surface, respectively. Gibbs adsorption equation states that

$$\frac{\partial \sigma}{\partial c_1} = -RT \frac{c_\Gamma}{c_1}, \tag{11.17}$$

and analogously for c_2, where RT is gas constant times temperature. The functional dependence between c_Γ and c_1, c_2 is also called isotherm and depends on the underlying assumptions of the considered physical system. The two most important isotherms are the laws of Henry and Langmuir, discussed in the next sections.

The evolution of surfactant concentrations c_1, c_2 and c_Γ can be determined by additional equations in the bulk phases and on the surface. Phase field modeling provides an easy way to account for such equations by use of the characteristic functions χ_1, χ_2 and δ indicating phase 1, phase 2 and the surface, respectively. A popular choice to approximate these functions in the diffuse interface context is

$$\chi_1 = \frac{1 + \phi}{2}, \qquad \chi_2 = \frac{1 - \phi}{2}, \qquad \delta = \frac{1}{2}|\nabla \phi|. \tag{11.18}$$

By use of these characteristic functions, equations given in one of the bulk domains or on the surface, can be extended to the full computational domain Ω which greatly simplifies their discretization. To illustrate this, let us consider a surface advection equation

$$\partial_t c_\Gamma + \nabla_\Gamma \cdot (\mathbf{v} c_\Gamma) = 0 \qquad \text{on } \Gamma, \tag{11.19}$$

which describes mass conservation of the concentration c_Γ on the surface. Now multiply with a test function ψ and integrate over Γ to obtain the weak form of this equation. Subsequently, we can conclude

$$\int_\Gamma \partial_t c_\Gamma \psi + \nabla_\Gamma \cdot (\mathbf{v} c_\Gamma) \psi = d_t \int_\Gamma c_\Gamma \psi - \int_\Gamma c_\Gamma \partial_t^\bullet \psi \qquad \text{(Leibnitz rule)}$$

$$= d_t \int_\Omega c_\Gamma \delta \psi - \int_\Omega c_\Gamma \delta \partial_t^\bullet \psi \qquad \text{(delta function)}$$

$$= \int_\Omega \partial_t (c_\Gamma \delta) \psi - \int_\Omega c_\Gamma \delta \mathbf{v} \cdot \nabla \psi \qquad \text{(since } \partial_t \psi = 0)$$

$$= \int_\Omega \partial_t (c_\Gamma \delta) \psi + \nabla \cdot (c_\Gamma \delta \mathbf{v}) \psi.$$

The strong form of the latter expression is,

$$\partial_t(\delta c) + \nabla \cdot (\delta c \mathbf{v}) = 0 \qquad \text{in } \Omega. \qquad (11.20)$$

Hence, Eq. (11.20) provides an extended form of the surface advection equation (11.19) that is now valid in the whole domain Ω.

Similar reformulations can be done for a large variety of bulk and surface equations, see [42, 52] for examples and justification by matched asymptotic analysis. In the following, we will focus on such diffuse interface formulations for the mass balance equations for the surfactants. The detailed form of these equations depends on the chosen isotherm. We refer to [27] for an overview of different adsorption isotherms and the corresponding diffuse interface formulations for two-phase flow with soluble surfactants.

11.2.4.1 The Henry Model

Based on experimental findings the Henry model assumes that the amount of molecules that are adsorbed at an interface is proportional to the concentration of these molecules in the ambient bulk phase [35]. This condition, also called Henry's law, means mathematically that the concentrations in the bulk phases, c_1, c_2, and on the interface, c_Γ, are related by the Henry constants H, H_Γ as follows:

$$c_2 = Hc_1, \qquad c_\Gamma = H_\Gamma c_1 \qquad \text{on } \Gamma. \qquad (11.21)$$

This condition allows to define a single continuous field $c : \Omega \to \mathbb{R}_{\geq 0}$ describing the surfactant concentration in the whole domain by

$$c_1 = c_{|\bar{\Omega}_1}, \qquad c_2 = Hc_{|\bar{\Omega}_2}, \qquad c_\Gamma = H_\Gamma c_{|\Gamma}, \qquad (11.22)$$

Consequently, the total surfactant mass can be expressed as $\int_\Omega [\chi_1 + \chi_2 H + \delta H_\Gamma] c \, dV$ and one can derive the mass balance equation,

$$\partial_t^\bullet ([\chi_1 + \chi_2 H + \delta H_\Gamma] c) - \nabla \cdot ([\chi_1 D_1 + \chi_2 H D_2 + \delta H_\Gamma D_\Gamma] \nabla c) = 0, \qquad (11.23)$$

where D_1, D_2, D_Γ are the diffusion constants in the corresponding phases. Approximating the characteristic functions by Eq. (11.18) allows to handle the surfactant concentrations in the two phases and on the interface by solving a single equation.

Henry's law together with Gibb's isotherm (11.17) yields the surfactant-dependent surface tension

$$\sigma = \sigma_0 - RT \, H_\Gamma c. \qquad (11.24)$$

Hence, Eqs. (11.3)–(11.6), (11.23)–(11.24) form a coupled system for two-phase flow with soluble surfactants.

The underlying assumptions restrict the use of Henry's law to situations of very low surface concentrations. However, due to its simplicity the model is still widely used and, even if further simplified, can explain many complicated flow phenomena. For example, in [54] it is assumed that surfactants do not dissolve in phase 2 ($H = 0$) and that interfacial adsorption is very low ($H_\Gamma \approx 0$). Still, the model was able to explain and qualitatively describe the surprising relaxation oscillations that occur at droplet surfaces exposed to an ambient fluid with a surfactant gradient.

11.2.4.2   Langmuir Model

The Langmuir model is probably the most popular adsorption isotherm. It can be derived from statistical physics and provides not only a stationary isotherm but also a rate of exchange between surfactant molecules in the bulk and on the surface. Accordingly, the flux from phase i to the surface is defined by

$$j_i := a_i c_i (1 - c_\Gamma/c_\infty) - d_i c_\Gamma \qquad\qquad i = 1, 2. \qquad\qquad (11.25)$$

Here, a_i, d_i are adsorption and desorption rates and the saturation constant c_∞ defines the concentration of maximal interface coverage. The mass balance equations for the phase-dependent surfactant concentrations become,

$$\partial_t^\bullet(\chi_i c_i) - D_i \nabla \cdot (\chi_i \nabla c_i) = -\delta j_i \qquad\qquad i = 1, 2, \qquad\qquad (11.26)$$

$$\partial_t^\bullet(\delta c_\Gamma) - D_\Gamma \nabla \cdot (\delta \nabla c_\Gamma) = \delta(j_1 + j_2). \qquad\qquad (11.27)$$

Evaluating the Gibbs isotherm (11.17) at equilibrium ($j_1 = j_2 = 0$) yields the surfactant-dependent surface tension

$$\sigma = \sigma_0 + RT c_\infty \ln(1 - c_\Gamma/c_\infty). \qquad\qquad (11.28)$$

Hence, Eqs. (11.3)–(11.6), (11.25)–(11.28) compose a diffuse interface model for two-phase flows with soluble surfactants based on the Langmuir isotherm.

In reality, also the Langmuir isotherm is limited by some underlying assumptions. In particular it accounts only for a monolayer of interfacial surfactants which is often doubtful as frequently more molecules adsorb to the monolayer. However, despite its limitations, Langmuir's isotherm is often the first choice for many practical applications.

The model has been used to describe soluble surfactants on droplets [55] and for Taylor bubbles, see the corresponding Chapter of this book [10]. An improved thermodynamically consistent form has been proposed and tested in [27]. In [8] the model was adapted for elastic interfacial nano-particles. There, c defines a particle number density instead of a concentration and elastic particle interactions give rise to additional surface forces.

11.3 Phase Field Models for Fluidic Elastic Membranes

Fluid membranes are one of the essential building blocks of biological cells. They separate the interior of all cells from the outside environment and divide intracellular regions into different functional compartments. The membrane itself consists of a dense bilayer of lipid molecules (and other proteins) and is mostly impermeable for fluids, see Fig. 11.2.

Although, the mathematical description by a phase field is identical to previous case of two-phase flow with surfactants, the dense packing of the lipids along the membrane gives now rise to elastic properties. Assuming the membrane to behave like a thin elastic shell leads to two essential elastic contributions: the membranes tendency to assume a preferred curvature (bending stiffness) and its tendency to locally conserve its surface area (inextensibility). In the following we will discuss how these constraints can be included in phase field models.

11.3.1 Bending Stiffness

In separated pioneering work, Helfrich [34] and Canham [17] assumed a Hookean response of the membrane to bending and derived the bending energy, also called Helfrich or Canham-Helfrich energy,

$$E_B = \int_\Gamma \frac{1}{2} k_B (H - H_0)^2 \, \mathrm{dA}. \tag{11.29}$$

Here, k_B is the bending stiffness, H the total curvature and H_0 the preferred curvature of the membrane. For a homogeneous lipid bilayer $H_0 = 0$.

Given a phase field that describes the membrane position, curvature as well as the interface delta function can be expressed in terms of ϕ, which allows to define the a
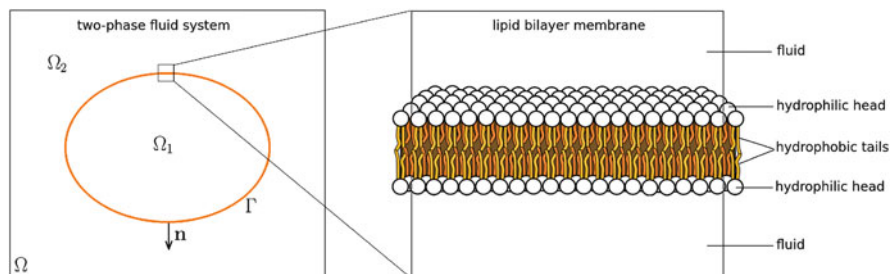
Fig. 11.2 Illustration of a closed fluid membrane. *Left*: Sharp interface setting, the membrane surface Γ separates two fluid phases Ω_1 and Ω_2. *Right*: A close-up shows the physical form of the membrane as a lipid bilayer. Image adapted from [4]

phase field variant of the bending energy. Du et al. proposed the following energy,

$$\tilde{E}_B = \int_\Omega \frac{3k_B}{8\sqrt{2}\varepsilon} \left(\varepsilon \Delta \phi - \frac{1}{\varepsilon} W_0'(\phi) \right)^2 dV, \tag{11.30}$$

where $W_0'(\phi) = (\phi^2 - 1)(\phi + \sqrt{2}\varepsilon H_0)$ is the first derivative of a modified double well potential [22]. In [21] and more rigorous in [57] convergence of $\tilde{E}_B$ toward the sharp interface bending energy E_B was shown as $\varepsilon \to 0$.

Early phase field methods for biomembranes were used without the coupling to hydrodynamics of the surrounding fluids. Such models were subject of numerical studies to describe equilibrium shapes of vesicles [20, 23] as well as analytical studies on existence and convergence of the proposed equations [19, 22]. Topological considerations including the calculation of the Euler number are addressed in [23, 25]. Reviews of existing phase field models for the minimization of the Helfrich energy can be found in [18, 41].

The coupling of the membrane dynamics with the fluid flow is typically derived by an energy variation approach. The resulting Navier-Stokes equations with additional bending stiffness force are [9, 24],

$$\rho \partial_t^\bullet \mathbf{v} + \nabla p - \nabla \cdot \left(\eta(\nabla \mathbf{v} + \nabla \mathbf{v}^T) \right) = -\varepsilon \nabla \cdot (\sigma \nabla \phi \otimes \nabla \phi) + \frac{\delta \tilde{E}_B}{\delta \phi} \nabla \phi, \tag{11.31}$$

$$\nabla \cdot \mathbf{v} = 0, \tag{11.32}$$

where the surface tension σ acts now as a Lagrange multiplier to enforce inextensibility, see Sect. 11.3.2. Further

$$\frac{\delta \tilde{E}_B}{\delta \phi} = \frac{3k_B}{4\sqrt{2}} \left[\frac{1}{\varepsilon^2} \mu W_0''(\phi) - \Delta \mu \right], \tag{11.33}$$

$$\mu = \frac{1}{\varepsilon} W_0'(\phi) - \varepsilon \Delta \phi. \tag{11.34}$$

Additionally, the phase field needs to be advected with the flow which is usually realized by an advected Willmore flow equation with or without volume conservation,

$$d_t \phi + \mathbf{v} \cdot \nabla \phi = -M \frac{\delta \tilde{E}_B}{\delta \phi} \qquad \text{(non-conserved)}, \tag{11.35}$$

$$d_t \phi + \mathbf{v} \cdot \nabla \phi = \nabla \cdot \left(M \nabla \frac{\delta \tilde{E}_B}{\delta \phi} \right) \qquad \text{(conserved)}. \tag{11.36}$$

Both choices for the advection of ϕ ensure thermodynamic consistency in the case of matched densities. Other approaches to advect the phase field include the advected field approach [11, 12] where a modified Allen-Cahn equation is used.

For the system of equations (11.31)–(11.35) without surface tension and inextensibility, existence of global weak solutions and uniqueness under extra regularity were proven [24]. Local time existence and uniqueness of strong solutions is shown in Liu et al. [43].

11.3.2 Inextensibility

The presence of the lipid molecules at the interface introduces a local inextensibility constraint, since the lipids resist interfacial compression and stretching. The local form of the inextensibility constraint reads

$$\nabla_\Gamma \cdot \mathbf{v} = 0, \tag{11.37}$$

which describes a surface incompressibility, similar to the bulk incompressibility condition in the fluid. The necessary Lagrange multiplier to enforce this condition, σ, enters Eq. (11.31) as a surface tension force, similar to the pressure in the Navier-Stokes equation to enforce incompressibility. Different approaches have been presented to realize the inextensibility constraint in phase field models. In the following we discuss and compare the approaches given in [4, 9, 12, 13, 24].

Global Inextensibility (Model A) In [24] the local inextensibility constraint is approximated by a weaker global constraint, i.e., a global conservation of surface area. To realize this, a penalty method is proposed and the total energy of the system is augmented by the penalty term

$$E_p = \frac{k_p}{2}(\mathscr{A}(\phi) - \mathscr{A}_0)^2, \tag{11.38}$$

$$\mathscr{A}(\phi) = \int_\Omega \frac{\varepsilon}{2}|\nabla\phi|^2 + \frac{1}{\varepsilon}W(\phi)\mathrm{dV}, \tag{11.39}$$

where $\mathscr{A}_0$ is the initial value of $\mathscr{A}(\phi)$. The corresponding global surface tension is

$$\sigma = k_p(\mathscr{A}(\phi) - \mathscr{A}_0), \tag{11.40}$$

which is positive if the surface area $\mathscr{A}(\phi)$ is too big and negative if $\mathscr{A}(\phi)$ is too small. The approach ensures conservation of the surface area given the factor k_p is large enough. A similar approach with penalty terms coupled to Lagrange multipliers has been presented in [23] and gives identical results for large k_p. In [9] it has been shown that the global and local inextensibility constraints may lead to significantly different membrane dynamics. In particular for situations of multiple approaching membranes the global constraint is not a good approximation and may lead to incorrect flow dynamics.

Local Inextensibility (Model B) A phase field model to account for the full local inextensibility, has been proposed in [9]. Therefore, the following regularized

extension of the inextensibility constraint over the whole domain was introduced,

$$\xi\varepsilon^2\nabla\cdot\left(\phi^2\nabla\sigma\right) + |\nabla\phi|\tilde{\nabla}_\Gamma\cdot\mathbf{v} = 0, \tag{11.41}$$

where the diffuse inextensibility constraint is defined as

$$\tilde{\nabla}_\Gamma\cdot\mathbf{v} = -\mathbf{n}\cdot\nabla\mathbf{v}\cdot\mathbf{n}. \tag{11.42}$$

Here, $\mathbf{n} = \nabla\phi/|\nabla\phi|$ represents the membrane normal, ξ is a regularization parameter independent of ε. Eq. (11.41) becomes $\tilde{\nabla}_\Gamma\cdot\mathbf{v} = \nabla_\Gamma\cdot\mathbf{v} = 0$ at the interface where $\phi \approx 0$, and reduces to $\Delta\sigma = 0$ away from Γ since $\phi^2 \approx 1$ and $|\nabla\phi| \approx 0$. This provides a harmonic extension of σ off Γ, while maintaining the local inextensibility constraint near Γ. Eq. (11.41) and the Navier-Stokes equation are coupled implicitly to determine velocity and surface tension simultaneously. The formulation of diffuse inextensibility is validated by asymptotic analysis and numerical tests in [9]. In [47] the model has been used to simulate the interaction between red and white blood cells within a blood vessel.

Local Inextensibility with Relaxation (Model C) The use of the regularization term in Eq. (11.41) can introduce small errors that may accumulate over time and thus lead to spurious local stretching and compression of the membrane. To correct these errors and drive a slightly stretched or compressed surface back to equilibrium, a relaxation mechanism has been proposed in [9]. A field c is introduced to measure local stretching of the interface. Setting the initial value $c(\mathbf{x}, 0) = 1$ and taking c to evolve by a surface mass conservation equation (11.19), locations where c deviates from 1 represent regions of compression ($c > 1$) or stretching ($c < 1$). As seen earlier the surface mass conservation equation can be approximated in the diffuse interface context by use of the characteristic delta function $\delta = |\nabla\phi|$. Additional normal diffusion ensures that the concentration is constantly extended off the interface and leads to the evolution equation

$$\partial_t(|\nabla\phi|c) + \nabla\cdot(|\nabla\phi|c\mathbf{v}) - D_n\nabla\cdot(|\nabla\phi|\mathbf{n}\,\mathbf{n}\cdot\nabla c) = 0. \tag{11.43}$$

Here, D_n is the normal diffusion constant and the use of $|\nabla\phi|$ in the diffusion operator ensures that the bulk concentration does not influence the surface concentration.

Hooke's law can be used to relax the local changes in interfacial area, which amounts in replacing the inextensibility constraint by $\nabla_\Gamma\cdot\mathbf{v} = \zeta(c-1)/c$ for a relaxation constant ζ. Within the diffuse interface formulation this means replacing Eq. (11.41) by

$$\xi\varepsilon^2\nabla\cdot\left(\phi^2\nabla\sigma\right) + |\nabla\phi|\tilde{\nabla}_\Gamma\cdot\mathbf{v} = \zeta|\nabla\phi|(c-1)/c, \tag{11.44}$$

The inextensibility with relaxation has been proven very effective with almost zero stretching and compression of the membrane [9]. Recently, the model has been applied to simulate the formation of a membrane vesicle from a larger

membrane during endocytosis [46]. There, curvature-inducing molecules sit on a part of the membrane and induce strong tangential forces which makes the process strongly dependent on the accuracy of the inextensibility constraint. Due to the size difference between the forming vesicle and the large membrane, only a part of the latter is considered and a special boundary condition for c is applied to regulate the influx of membrane area from the domain boundary.

Inextensibility from Membrane Stretch Elasticity (Model D) An alternative approach can be constructed from the physical origin of the membrane inextensibility, namely the membrane stretch energy. Assuming a Hookean response of lipid molecules against compression and stretching leads to the additional stretch energy

$$E_{\text{stretch}} = \int_\Gamma \frac{1}{2} k_s (J-1)^2 \mathrm{dA}, \tag{11.45}$$

where J is the local area stretch of the membrane and k_s the stretching modulus. The local area stretch J is defined as the current area of a surface element divided by the initial area of the same material part of the surface: $J = A/A_0$, hence, $J = 1$ corresponds to the reference state [4].

The above energy was already present in the famous paper of Helfrich [34] and leads, in first order, to a surface tension

$$\sigma = k_s(J-1), \tag{11.46}$$

see [4]. The common inextensibility constraint and corresponding surface tension can actually be seen as approximations to this stretching tension for very large k_s.

The evolution of the local area stretch is determined by the surface evolution equation

$$d_t J + \mathbf{v} \cdot \nabla J = J \nabla_\Gamma \cdot \mathbf{v} \qquad \text{on } \Gamma. \tag{11.47}$$

However it might be more favorable to introduce the inverse of the stretch, $c = 1/J$, which leads to a conservative evolution

$$d_t c + \nabla_\Gamma \cdot (\mathbf{v}c) = 0 \qquad \text{on } \Gamma. \tag{11.48}$$

Approximating this with a diffuse interface model results in Eq. (11.43) again, but contrary to model C this equation is now used to provide the surface tension directly [without involving Eq. (11.44)]. Accordingly, from Eq. (11.46) we obtain $\sigma = k_s(1-c)/c$.

The model is quite similar to the approach described in [12, 13], where a non-conserved evolution equation for c was used. However, the conservation property of Eq. (11.43) is quite desirable since it can be carried over to the discretized model and hence ensures highly accurate conservation of the local membrane area for all times.

11.3.3 Model Comparison

In the following, we perform numerical simulations to test models A, B, C and D in two dimensions. Therefore, the conserved Willmore flow equation (11.36) is coupled to the Navier-Stokes equation (11.31)–(11.32) and the respective inextensibility constraint. We simulate shear flow around a single elliptical vesicle and compare the four models in terms of vesicle dynamics and accuracy of the inextensibility constraint.

Discretization and Parameters We use a Finite-Element discretization with semi-implicit Euler timestepping. P2 elements are used to discretize the velocity, phase field, chemical potential and concentration while the pressure is discretized with P1 elements. Details on the discretization of the Willmore and Navier-Stokes problem can be found in [9], the handling of the surface equation (11.43) for c is described in [46].

A vesicle with major axis of length $45\,\mu$m and minor axis of length $15\,\mu$m is placed in the center of a domain $\Omega = [0, 60\,\mu\text{m}]^2$. We prescribe a shear rate of 0.2s^{-1} at the domain boundary. Typical experimental parameters are used for density, $\rho_2 = 10^3\,\text{kg/m}^3, \rho_1 = 1.125\rho_2$, viscosity $\eta_2 = 10^{-3}\text{Pa s}, \eta_1 = 20\eta_2$, spontaneous curvature $H_0 = 0$ and bending stiffness $k_B = 10^{-19}\,\text{Nm}$.

The mobility $M = 5 \cdot 10^{-12}\,\text{m}^3\text{s/kg}$ is chosen small enough that the interface is primarily advected. The parameters for model B and C are discussed further in [9], here we use $\xi = 1.33 \cdot 10^4\,\text{m}^{-1}\text{s}^{-1}, \zeta = 20\,\text{s}^{-1}, D_n = 3 \cdot 10^{-5}\,\text{m/s}$. The penalty coefficient, $k_p = 3 \cdot 10^4\,\text{N/m}^3$, and stretching coefficient, $k_s = 6.8 \cdot 10^{-6}\,\text{N/m}$, are chosen large enough to guarantee proper global and local inextensibility, respectively. Finally, the time step size is $\tau = 5\,\text{ms}$, the interface thickness is $\varepsilon = 0.45\,\mu$m and the spatial mesh is adaptive with a minimum grid size of $h = 0.5\,\mu$m around the interface. Note that this ensures a resolution of approximately 7 degrees of freedom across the interface, since the corresponding thickness of the interface region (where $-0.9 < \phi < 0.9$) is $1.87\,\mu$m and due to the use of P2 elements.

The use of the conserved Willmore equation (11.36) already leads to a very good conservation of vesicle volume. To ensure even perfect volume conservation we add a growth relaxation term. To this end, we specify the vesicle volume as $\mathcal{V} = \int_\Omega (\phi + 1)/2\text{dV}$ and denote the initial value of $\mathcal{V}$ by $\mathcal{V}_0$. The term $|\nabla\phi|(\mathcal{V}_0 - \mathcal{V})$ is added to the left-hand side of Eq. (11.36) aiming to compensate small changes in vesicle volume by growing or shrinking the vesicle around the interface. Note that the restriction of this growth to the interface can be derived from the corresponding sharp interface volume constraint. This restriction is an essential difference to other models which simply add constant values to the phase field to conserve the integral of the phase field, e.g. in [9, 23, 24, 47].

11.3.3.1 Inextensibility Test

As seen in Fig. 11.3, the vesicle volume and the total interface area are conserved very well for all four models. Model B exhibits the largest errors of up to 0.16%, which is still very small. Note, that the area conservation in model B is a pure result of a diffusely inextensible velocity field since there is no relaxation mechanism. To reduce the small error further, a global area conservation mechanism as in model A can be added to model B, like proposed in [9, 47]. For the vesicle volume, we find extremely good conservation due to the above growth relaxation term. Without this term a slight volume loss of up to 0.1% is observed.

The accumulated stretching is presented in Fig. 11.4. To this end, the value of the concentration c is plotted over the arc length of the interface at time $t = 35$ s,
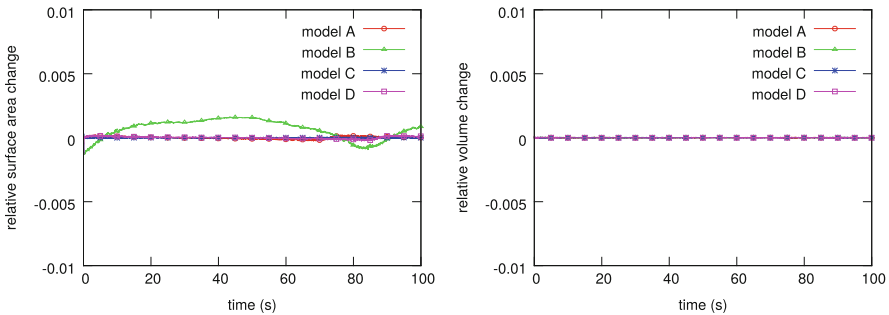

Fig. 11.3 Relative change in vesicle surface area (*left*) and volume (*right*) over time. The relative change in surface area is measured by $(\mathscr{A}(\phi) - \mathscr{A}_0)/\mathscr{A}_0$, the relative change in vesicle volume is $(\mathscr{V}(\phi) - \mathscr{V}_0)/\mathscr{V}_0$. All models show very good global conservation. Errors in surface area are less than 0.2%, errors in volume are less than 0.01%
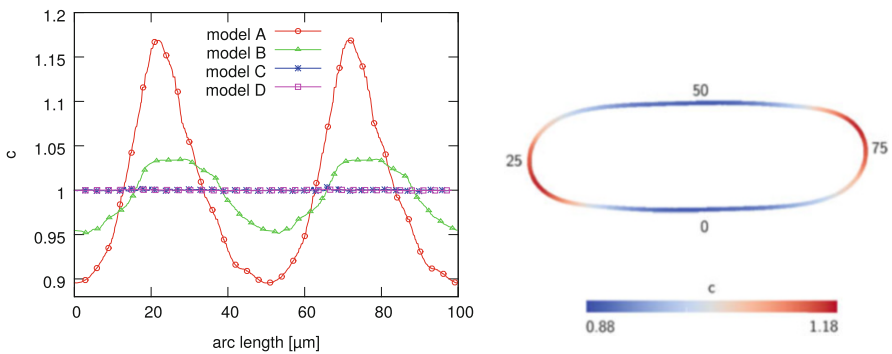
Fig. 11.4 The accumulated local stretching at $t = 35$ s. *Left*: The concentration c over the arc length of the interface. Model A exhibits interfacial stretching of up to 17%, model B reduces local stretching/compression significantly, models C and D show perfect inextensibility ($c = 1$). *Right*: Spatial distribution of c along the interface for model A showing compression at the tips and stretching along the sides. Numbers around the vesicle indicate the arc length
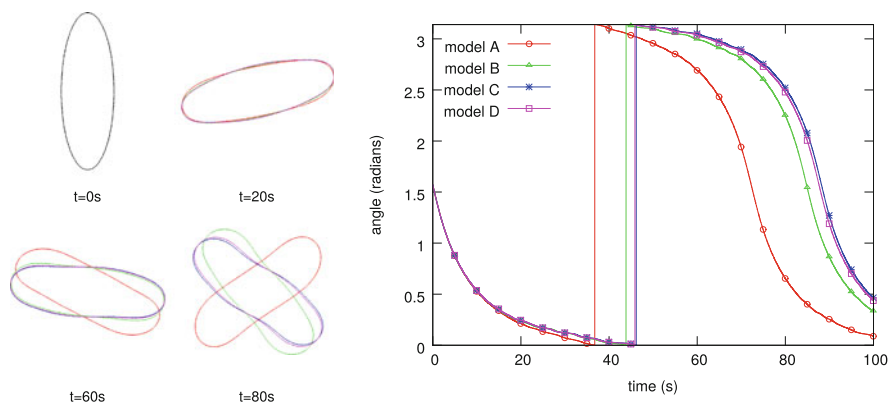
Fig. 11.5 Vesicle shapes (*left*) and inclination angles (*right*) over time. The local inextensibility constraints in models B, C, D significantly delays the tumbling time as compared to model A. Models C and D give almost identical results

when the vesicle is in all models in an almost horizontal state. Note, that the total length of the initial elliptical vesicle is almost exactly $100\,\mu$m. For Model A we find strong interface compression (up to 17%) around the tips of the vesicle while the sides of the vesicle are stretched (up to 11%). This behavior was also observed in [9]. The local inextensibility constraint in models B,C,D suppresses these compression/stretching errors. In particular models C and D show absolutely no local stretching or compression. The relatively large values for model B are actually inherited from the first time steps and might result from the slight interfacial stretching and compression during the initial equilibration of the interface.

11.3.3.2 Model Comparison

The time evolution of the vesicle shapes and the corresponding inclination angles are depicted in Fig. 11.5. For the given parameter set, the vesicle is in the tumbling regime. We find that the vesicle rotates significantly faster in model A than in the locally inextensible models. While models C and D lead to almost identical evolutions, the vesicle dynamics is slightly accelerated in model B.

We conclude that the accurate incorporation of local inextensibility is important to obtain reliable vesicle dynamics in numerical simulations. The global inextensibility constraint in model A is not sufficient and leads to accelerated vesicle dynamics in shear flow. The inextensible models B, C and D provide much more accurate solutions, in particular models C and D seem to completely eliminate local stretching or compression. From a numerical point of view, models B and C are typically coupled monolithically to the Navier-Stokes equation, which makes these models very stable. For model B also energy laws can be shown, see [9] for the matched density case. Model D is explicitly coupled to the Navier-Stokes

equations which compromises the stability, hence, for large k_s time step constraints will appear. However, for moderate k_s, model D provides a simple and yet very effective numerical model for highly accurate local inextensibility. Since model D is based on the stretching energy (11.45), it might be possible to derive energy stable numerical schemes for this model as well.

References

1. Abels, H., Garcke, H., Grün, G.: Thermodynamically consistent, frame indifferent diffuse interface models for incompressible two-phase flows with different densities. Math. Models Methods Appl. Sci. **22**(3) (2012). doi:10.1142/S0218202511500138

2. Aland, S.: Modelling of two-phase flow with surface-active particles. Dissertation, TU Dresden (2012)

3. Aland, S.: Time integration for diffuse interface models for two-phase flow. J. Comput. Phys. **262**, 58–71 (2014). doi:10.1016/j.jcp.2013.12.055

4. Aland, S.: Phase field modeling of inhomogeneous biomembranes in flow. In: Becker, S. (ed.) Microscale Transport Modelling in Biological Processes, chap. 9. Elsevier, Amsterdam (2016)

5. Aland, S., Chen, F.: An efficient and energy stable scheme for a phase-field model for the moving contact line problem. Int. J. Numer. Methods Fluids **81**(11), 657–671 (2015). doi:10.1002/fld.4200

6. Aland, S., Voigt, A.: Benchmark computations of diffuse interface models for two-dimensional bubble dynamics. Int. J. Num. Meth Fluids **69**, 747–761 (2012). doi:10.1002/fld.2611

7. Aland, S., Lowengrub, J.S., Voigt, A.: Two-phase flow in complex geometries: a diffuse domain approach. CMES **57**(1), 77–106 (2010)

8. Aland, S., Lowengrub, J., Voigt, A.: A continuum model of colloid-stabilized interfaces. Phys. Fluids **23**(6), 062103 (2011). doi:10.1063/1.3584815

9. Aland, S., Egerer, S., Lowengrub, J., Voigt, A.: Diffuse interface models of locally inextensible vesicles in a viscous fluid. J. Comput. Phys. **277**, 32–47 (2014). doi:10.1016/j.jcp.2014.08.016

10. Aland, S., Hahn, A., Kahle, C., Nürnberg, R.: Comparative simulations of Taylor-flow with surfactants based on sharp- and diffuse-interface methods. In: Reusken, A., Bothe, D. (eds.) Advances in Mathematical Fluid Mechanics. Springer, New York (2017)

11. Beaucourt, J., Rioual, F., Séon, T., Biben, T., Misbah, C.: Steady to unsteady dynamics of a vesicle in a flow. Phys. Rev. E **69**(1), 011906 (2004)

12. Biben, T., Misbah, C.: Tumbling of vesicles under shear flow within an advected-field approach. Phys. Rev. E **67**(3), 31908 (2003). doi:10.1103/PhysRevE.67.031908

13. Biben, T., Kassner, K., Misbah, C.: Phase-field approach to three-dimensional vesicle dynamics. Phys. Rev. E **72**(4), 41921 (2005). doi:10.1103/PhysRevE.72.041921

14. Boyanova, P., Do-Quang, M., Neytcheva, M.: Efficient preconditioners for large scale binary Cahn-Hilliard models. Comput. Methods Appl. Math. **12**(1), 1–22 (2012). doi:10.2478/cmam-2012-0001

15. Boyer, F.: A theoretical and numerical model for the study of incompressible mixture flows. Comput. Fluids **31**(1), 41–68 (2002)

16. Cahn, J.W., Hilliard, J.E.: Free energy of a nonuniform system. I. Interfacial free energy. J. Chem. Phys. **28**(2), 258–267 (1958)

17. Canham, P.B.: The minimum energy of bending as a possible explanation of the biconcave shape of the human red blood cell. J. Theor. Biol. **26**(1), 61–81 (1970)

18. Du, Q.: Phase field calculus, curvature-dependent energies, and vesicle membranes. Philos. Mag. **91**(1), 165–181 (2011)
19. Du, Q., Zhu, L.: Analysis of a mixed finite element method for a phase field bending elasticity model of vesicle membrane deformation. J. Comput. Math. **24**(3), 265–280 (2006)
20. Du, Q., Liu, C., Wang, X.: A phase field approach in the numerical study of the elastic bending energy for vesicle membranes. J. Comput. Phys. **198**(2), 450–468 (2004)
21. Du, Q., Liu, C., Ryham, R., Wang, X.: Modeling the spontaneous curvature effects in static cell membrane deformations by a phase field formulation. Commun. Pure Appl. Anal. **4**(3), 537–548 (2005)
22. Du, Q., Liu, C., Ryham, R., Wang, X.: A phase field formulation of the Willmore problem. Nonlinearity **18**, 1249–1267 (2005). doi:10.1088/0951-7715/18/3/016
23. Du, Q., Liu, C., Wang, X.: Simulating the deformation of vesicle membranes under elastic bending energy in three dimensions. J. Comput. Phys. **212**(2), 757–777 (2006)
24. Du, Q., Li, M., Liu, C.: Analysis of a phase field Navier-Stokes vesicle-fluid interaction model. Discrete Continuous Dyn. Syst. **8**(3), 539–556 (2007)
25. Esedoglu, S., Rätz, A., Röger, M.: Colliding interfaces in old and new diffuse-interface approximations of willmore-flow. Commun. Math. Sci. **12**(1), 125–147 (2013). doi:10.4310/CMS.2014.v12.n1.a6
26. Feng, X.: Fully discrete finite element approximations of the Navier–Stokes–Cahn-Hilliard diffuse interface model for two-phase fluid flows. SIAM J. Numer. Anal. **44**, 1049–1072 (2006). doi:10.1137/050638333
27. Garcke, H., Lam, K., Stinner, B.: Diffuse interface modelling of soluble surfactants in two-phase flow. Commun. Math. Sci. **12**(8), 1475–1522 (2014)
28. Garcke, H., Hinze, M., Kahle, C.: A stable and linear time discretization for a thermodynamically consistent model for two-phase incompressible flow. Appl. Numer. Math. **99**, 151–171 (2016). doi:10.1016/j.apnum.2015.09.002
29. Grün, G.: On convergent schemes for diffuse interface models for two-phase flow of incompressible fluids with general mass densities. {SIAM} J. Numer. Anal. **51**(6), 3036–3061 (2013). doi:10.1137/130908208
30. Grün, G., Klingbeil, F.: Two-phase flow with mass density contrast: stable schemes for a thermodynamic consistent and frame-indifferent diffuse-interface model. J. Comput. Phys. **257**, 708–725 (2014). doi:10.1016/j.jcp.2013.10.028
31. Guillén-González, F., Tierra, G.: On linear schemes for a Cahn–Hilliard diffuse interface model. J. Comput. Phys. **234**, 140–171 (2013). doi:10.1016/j.jcp.2012.09.020
32. Han, D., Wang, X.: A second order in time, uniquely solvable, unconditionally stable numerical scheme for Cahn–Hilliard–Navier–Stokes equation. J. Comput. Phys. **290**, 139–156 (2015). doi:10.1016/j.jcp.2015.02.046
33. He, Q., Glowinski, R., Wang, X.P.P.: A least-squares/finite element method for the numerical solution of the {Navier-Stokes-Cahn-Hilliard} system modeling the motion of the contact line. J. Comput. Phys. **230**(12), 4991–5009 (2011). doi:10.1016/j.jcp.2011.03.022
34. Helfrich, W.: Elastic properties of lipid bilayers: theory and possible experiments. Zeitschrift fur Naturforschung. Teil C: Biochemie, Biophysik, Biologie, Virologie **28**(11), 693–703 (1973). doi:10.1002/mus.880040211
35. Henry, W.: Experiments on the quantity of gases absorbed by water, at different temperatures, and under different pressures. Philos. Trans. R. Soc. Lond. **93**, 29–276 (1803)
36. Hohenberg, P.C., Halperin, B.I.: Theory of dynamic critical phenomena. Rev. Mod. Phys. **49**(3), 435 (1977)
37. Jaqmin, D.: Calculation of two-phase Navier-Stokes flows using phase-field modelling. J. Comput. Phys. **155**, 96–127 (1999). doi:10.1006/jcph.1999.6332
38. Kay, D., Loghin, D., Wathen, A.: A preconditioner for the steady-state navier–stokes equations. SIAM J. Sci. Comput. **24**(1), 237–256 (2002)
39. Kay, D., Welford, R.: Efficient numerical solution of Cahn-Hilliard-Navier-Stokes fluids in 2D. SIAM J. Sci. Comput. **29**, 15–43 (2007). doi:10.1137/050648110

40. Kim, J.: A continuous surface tension force formulation for diffuse-interface models. J. Comput. Phys. **204**(2), 784–804 (2005). doi:10.1016/j.jcp.2004.10.032. http://linkinghub.elsevier.com/retrieve/pii/S0021999104004383
41. Lázaro, G.R., Pagonabarraga, I., Hernández-Machado, A.: Phase-field theories for mathematical modeling of biological membranes. Chem. Phys. Lipids **185**, 46–60 (2015)
42. Li, X., Lowengrub, J., Rätz, A., Voigt, A.: Solving PDEs in complex geometries: a diffuse domain approach. Commun. Math. Sci. **7**(1), 81–107 (2009)
43. Liu, Y., Takahashi, T., Tucsnak, M.: Strong solutions for a phase field Navier–Stokes vesicle–fluid interaction model. J. Math. Fluid Mech. **14**(1), 177–195 (2012)
44. Liu, C., Shen, J., Yang, X.: Decoupled energy stable schemes for a phase-field model of two-phase incompressible flows with variable density. J. Sci. Comput. **62**(2), 601–622 (2014). doi:10.1007/s10915-014-9867-4
45. Lowengrub, J., Truskinovsky, L.: Quasi-incompressible Cahn–Hilliard fluids and topological transitions. In: Proceedings of the Royal Society of London A: Mathematical, Physical and Engineering Sciences, vol. 454, pp. 2617–2654. The Royal Society, London (1998)
46. Lowengrub, J., Allard, J., Aland, S.: Numerical simulation of endocytosis: viscous flow driven by membranes with non-uniformly distributed curvature-inducing molecules. J. Comput. Phys. **309**, 112–128 (2016). doi:10.1016/j.jcp.2015.12.055
47. Marth, W., Aland, S., Voigt, A.: Margination of white blood cells - a computational approach by a hydrodynamic phase field model. J. Fluid Mech. **790**, 389–406 (2016)
48. Muradoglu, M., Tryggvason, G.: A front-tracking method for computation of interfacial flows with soluble surfactants. J. Comput. Phys. **227**(4), 2238–2262 (2008)
49. Pozrikidis, C.: Boundary Integral and Singularity Methods for Linearized Viscous Flow. Cambridge University Press, Cambridge (1992)
50. Qian, T., Wang, X.P., Sheng, P.: Molecular scale contact line hydrodynamics of immiscible flows. Phys. Rev. E **68**(1), 016306 (2003)
51. Rannacher, R.: Finite element methods for the incompressible Navier-Stokes equations. Ph.D. thesis (2000)
52. Rätz, A., Voigt, A.: PDE's on surfaces—a diffuse interface approach. Commun. Math. Sci. **4**(3), 575–590 (2006)
53. Rowlinson, J.: Translation of J.D. van der Waals' "The thermodynamik theory of capillarity under the hypothesis of a continuous variation of density". J. Stat. Phys. **20**(2), 197–200 (1979)
54. Schwarzenberger, K., Aland, S., Domnick, H., Odenbach, S., Eckert, K.: Relaxation oscillations of solutal Marangoni convection at curved interfaces. Colloids Surf. A **481**, 633–643 (2015)
55. Teigen, K.E., Song, P., Lowengrub, J., Voigt, A.: A diffuse-interface method for two-phase flows with soluble surfactants. J. Comput. Phys. **230**, 375 (2011)
56. Villanueva, W., Amberg, G.: Some generic capillary-driven flows. Int. J. Multiphase Flow **32**(9), 1072–1086 (2006). doi:10.1016/j.ijmultiphaseflow.2006.05.003
57. Wang, X.: Asymptotic analysis of phase field formulations of bending elasticity models. SIAM J. Math. Anal. **39**(5), 1367–1401 (2008). doi:10.1137/060663519
58. Wise, S., Kim, J., Lowengrub, J.: Solving the regularized, strongly anisotropic cahn–hilliard equation by an adaptive nonlinear multigrid method. J. Comput. Phys. **226**(1), 414–446 (2007)
59. Xu, J.J., Li, Z., Lowengrub, J., Zhao, H.: A level-set method for interfacial flows with surfactant. J. Comput. Phys. **212**(2), 590–616 (2006)
60. Zhang, J., Johnson, P.C., Popel, A.S.: An immersed boundary lattice Boltzmann approach to simulate deformable liquid capsules and its application to microscopic blood flows. Phys. Biol. **4**(4), 285 (2007)